Using a New Top-Down Constrained Emissions Inventory to Attribute the Previously Unknown Source of Extreme Aerosol Loadings Observed Annually in the Monsoon Asian Free Troposphere

Shuo Wang[1]*, Jason Blake Cohen[1,2,3]*, Weizhi Deng[1], Kai Qin[3], Jianping Guo[4]

[1] School of Atmospheric Sciences, Sun Yat-Sen University, Guangzhou, China

[2] Southern Marine Science and Engineering Guangdong Laboratory (Zhuhai), Zhuhai, China

[3]School of Environment and Geoinformatics, China University of Mining and Technology, Xuzhou, China

[4]State Key Laboratory of Severe Weather, Chinese Academy of Meteorological Sciences, Beijing, China

Correspondence to: Jason Blake Cohen (jasonbc@alum.mit.edu)

* These Authors Contributed Equally To This Work

Key Points:

- New constrained emissions provide the best daily to weekly scale model fit with independent measurements in space, time, and magnitude.
- Increases in BC emissions from 6.6 to 11.9 times are required to match the observed aerosol loadings in free tropospheric Monsoon Asia.
- A new spatiotemporal pathway is observed to transport aerosols far to both the southwest and east to match extreme aerosol events.

Abstract

The contribution of biomass burning to the total aerosol loading over Monsoon Asia is both significant while also continuing to increase in recent decades. To better match the spatio-temporal distribution of aerosols and trace gasses observed in the free troposphere, this work applied a 3-D constrained emission inventory based on top-down remotely sensed NO_2 measurement to investigate the most extreme of the annually occurring biomass burning seasons in Monsoon Asia. In 2016 this constituted an extreme event observed over a 6-day period covering millions of square kilometers, including over regions which are typically in the rainy phase of the Monsoon at this time. The results are shown to be consistent with respect to TRMM precipitation, AERONET measurements, MODIS AOD, MOPITT CO, and reanalysis meteorology, over both the biomass burning source as well as the millions of square kilometers downwind both to the East and to the Southwest. Reproducing the observed long-range transport pattern requires the time of biomass burning to be increased, regions not previously identified as burning to be actual source regions, and the emissions of BC to be 6.6 to 11.9 time larger than current inventories. The underlying mechanism for this long-range transport involves a new 3-D pathway that can occur during the transition from the North to the South Monsoon. The results are also consistent with the new idea that large loadings of BC in the lower free troposphere may significantly affect the meteorological field and the overall vertical distribution of aerosols in the tropical troposphere.

Plain Language Summary

A new top-down 3-D emission inventory based on NO_2 measurements is used to investigate the spatial-temporal distribution of extreme aerosol events spread over millions of square kilometers observed in March 2016, as confirmed by independent observations of aerosols, trace gasses, and precipitation. The results show a 6.6-11.9 times increase in BC emissions from known but underestimated and previously unidentified sources in Eastern India and Northern Southeast Asia. These new sources are required for models to successfully match extreme events measured over a 6-day period as far away as in Singapore, Malaysia, Sumatra, Taiwan and the Western Pacific. The transport pathway involves a complicated 3-D pathway of lofting to the free troposphere and interaction with the change in the East Asian Monsoon system. This work helps to understand how aerosols from new or mis-understood sources in South and Southeast Asia may ultimately lead to impacts on the environment both locally and thousands of kilometers away, and provides a pathway to analyze such previously untraceable events.

1 Introduction

Biomass burning makes a significant and continuously increasing contribution to the total aerosol emissions over the parts of South Asia, Southeast Asia, and East Asia impacted by the Asian Monsoon (Cohen et al., 2018; Jin & Wang, 2017; N.-H. Lin et al., 2013; Jeffrey S. Reid et al., 2013; van der Werf et al., 2017). Almost all of the extreme aerosol events in this region, including those in megacities are either directly or in part due to biomass burning (Cohen & Wang, 2014). Such extreme loadings of aerosols have a significant impact on the atmospheric composition, the climate (Tao et al., 2012), the ecosystem (J. S. Reid et al., 2005), and human health (Streets et al., 2003; C. Wang, 2013). Furthermore, the impact of biomass burning on the environment is very uneven in space and time, having both a strong periodicity (annual or bi-annual) as well as a high variability (inter-annual and intra-annual) (Cohen, 2014; Cohen et al., 2011; Kaufman et al., 2002), making the overall impacts stronger over shorter temporal scales (from days to weeks) as compared to those from urban sources(Deng et al., 2020; Gonzalez-Alonso et al., 2019).

Biomass burning emissions are a significant source of aerosols and trace gases, including Black Carbon (BC), Organic Carbon (OC), VOCs, CO, and NO_2, and indirectly contributing to ozone, secondary aerosols, and heat, which in turn generates buoyancy and associated ascending airflow (Aouizerats et al., 2015; Ramanathan & Carmichael, 2008). Hotter fires simultaneously generate more absorbing aerosols, stronger buoyancy, and a significant change in the NO_2/CO ratio, all of which in turn may combine to increase the height of the emissions plume as compared to any individual forcing alone (S. Wang et al., 2020). Under these conditions, a significant amount of the total plume mass will frequently reach the free troposphere (Cohen et al., 2018; Gonzalez-Alonso et al., 2019; S. Wang et al., 2020), from which these sources will subsequently spread further downwind, whereby any impact on the atmospheric energy balance, circulation, clouds and precipitation, and the tropospheric distribution will spread over larger spatial scales (Streets et al., 2003).

Trace gasses and aerosols take days to weeks to transport hundreds to thousands of kilometers downwind, during which time they continue to change due to in-situ physics and chemistry, leading to particle growth due to deposition of co-emitted semi-volatile species (Aouizerats et al., 2015; Singh et al., 2018), hydroscopic uptake of water (Chen et al., 2019; Tao et al., 2012), and coagulation (J. S. Reid et al., 2005). Furthermore, due to the large amount of

BC emitted by biomass burning, and the strong interactions between BC and solar radiation in this part of the world, enhanced interactions with visible radiation (Chung & Seinfeld, 2002; Ramanathan & Carmichael, 2008) especially as the aerosols continue to coat and age (Cohen et al., 2017; Cohen & Wang, 2014; S. Wang et al., 2020), should lead to greater overall stability and lifetime with respect to evaporation and cloud uptake (C. Wang, 2013). Accordingly, these aged aerosols tend to more strongly interact with visible radiation than more fresh particles (Chapman et al., 2009; Forkel et al., 2012; Grandey & Wang, 2019; Lau & Kim, 2006), leading to a stronger AOD and reduction in visibility per unit of aerosol mass, as well as other greater adverse effects on the environment and health (Abba et al., 2012; Pavagadhi et al., 2013).

In Eastern India and Continental Southeast Asia (Myanmar, Northern Thailand, Laos and Northern Vietnam, and to a lesser extent in Cambodia and Southern Vietnam) there has been recurring and widespread biomass burning events in terms of emissions and geographic distribution, due to a significant change in forest coverage (including biomass fuel combustion consumption as high as 20 kgC/m2) and rapid economic and agricultural development over the past decade (Rosenfeld et al., 2014; van der Werf et al., 2006). These events occur annually, although with a significant amount of inter-annual and intra-annual viability in terms of their start time, duration, and intensity (Cohen, 2014). There is some speculation that these events may be impacted by climate variability including ENSO and the Indian Ocean Dipole (As-syakur et al., 2014; Cohen et al., 2017; Field et al., 2009; Hong et al., 2008; Pan et al., 2018; J. S. Reid et al., 2012). The general climatology of these biomass burning events was previously thought to be confined geographically within Southeast Asia itself, or to possibly extend eastward to Hainan and Guangxi or westward to Bangladesh (Hyer & Chew, 2010; N.-H. Lin et al., 2014). This is due to the fact that the winds in February and March over this region tend to have an East-West Flow as the Asian Monsoon transitions from its North-South mode into its South-North mode (Chang et al., 2005), leading this region being very dry with low surface wind speeds and intense radiation, thereby experiencing many wild-fires (Aouizerats et al., 2015; Cohen, 2014; van der Werf et al., 2008). However, recent work has established that in fact these sources can transport a significant amount of aerosol and trace gasses throughout Southern Greater China, and beyond to have an impact on Eastern Asia (Cohen et al., 2017; C. Lin, Cohen, Wang, & Lan, 2020).

Due to the heavy rainfall experienced over the Maritime Continent during this time of year and coupled with a very weak North/South wind, there has never been any indication that these large biomass burning plumes were capable to advect up to 2000km to the south to have an impact on the Maritime Continent (Cohen et al., 2018; C. Wang, 2013). A detailed analysis the multi-year AERONET measurements in Southern Thailand (Songkla) and Malaysia (Penang), and decadal AERONET measurements in Singapore (Cohen & Wang, 2014) have never revealed any significant recurring aerosol events in this region during this time of the year. If any such transport were to occur in addition to the other issues raised, the highly variable topography would require a significant amount of aerosol lofting above the boundary layer, which present day models do not generally indicate occurs within Continental Southeast Asia (Xue et al., 2020). Furthermore, most of the remaining datasets over this region tend to be based on surface measurements, which therefore would also likely miss the above-the-boundary layer transport that occurred, if it occurred at all.

The current generation of atmospheric chemical transport models have been used to investigate the transport of biomass burning smoke in both Continental Southeast Asia and the Maritime Continent under the influence of El Niño and other meteorological factors (sea/land

breeze, trade wind, typhoon, and topography) during their respective dry and biomass burning periods (J. S. Reid et al., 2012; C. Wang, 2013). Some work has been able to obtain a good match with respect to ground-based observation of $PM_{2.5}$ (Le et al., 2020; Zhang et al., 2019), PM_{10} (Hyer & Chew, 2010; C. Wang, 2013), carbon monoxide (CO) (Jeffrey S. Reid et al., 2013; J. S. Reid et al., 2005), and ozone (Ding et al., 2013), within the respective sub-regions. However, to date, there has been no modeling study able to match the large-scale and coherent plumes in terms of space and time identified in Cohen (Cohen, 2014), Cohen et al. (Cohen et al., 2017), and Lin et al. (C. Lin, Cohen, Wang, & Lan, 2020; C. Lin, Cohen, Wang, Lan, et al., 2020) over these individual regions of the world in terms of magnitude, height, and duration. Furthermore, there is no modeling study found able to show a significant amount of transport from Continental Southeast Asia to the Maritime Continent (Jeffrey S. Reid et al., 2013). Yet, due to the complexity of the geography, meteorology, and dynamics, as well as intense cloud-cover in Southeast Asia, models provide an important component for improving the understanding of the sources and transport of aerosols over this region of the world (N.-H. Lin et al., 2013; J. S. Reid et al., 2012).

This work reproduces the observed aerosol profile over this region more successfully than previous studies i.e. a significant amount of aerosols as high as 600mb and advected as far as the Western Pacific (Aouizerats et al., 2015), by introducing a variance maximization technique based on remotely sensed measurements of AOD, NO_2 and CO to derive a unique top-down spatial and temporal representation of the biomass burning source emissions profile (Cohen, 2014; Cohen & Wang, 2014; C. Lin, Cohen, Wang, Lan, et al., 2020; S. Wang et al., 2020). The results of this method have been shown to be reliable over other biomass burning regions as well, based on comparison of the results against remotely sensed measurements not used to derive the emissions and AERONET and other surface measurement networks. There are 4 significant differences in the emissions underlying these findings: first, the total magnitude is larger; second the burning occurs over a wider spatial distribution including in mountains and forested areas; third there is a significant amount of mass emitted above the boundary layer; and finally there is an increase in the total number of burning days. These differences in turn are the underlying reasons why the end results match more closely with independent measurements. In specific, this approach shows that in 2016, there was a significant transport of aerosols from Continental Southeast Asia to the Maritime Continent and equator, directly impacting Southern Thailand, Peninsular Malaysia, Singapore, and Sumatra. At the same time the region suddenly shifted from what is typical very wet to being extremely dry, allowing for little to no removal of aerosols transported in this direction. These findings have been partially observed by a study using joint measurements of AOD, NO_2, and CO (C. Lin, Cohen, Wang, & Lan, 2020; Stavrakou et al., 2008; Tang et al., 2013), but have never previously been successfully modeled.

This work further raises the point that the intense amount of aerosols emitted and/or the heat from the biomass burning may themselves impact the atypical meteorology, in turn altering the ultimate transport pathway (Jin & Wang, 2017; J. S. Reid et al., 2016). Since biomass burning aerosols contain copious amounts of BC and partially absorbing OC, they absorb radiation, which in turn cause the local atmosphere to warm up, inducing changes in the vertical temperature distribution and the dynamics (Jin & Wang, 2017; Sato et al., 2003; Tao et al., 2012). A single recent paper has argued this is the case when the aerosols are exclusively trapped in the boundary layer over this part of the world (Xue et al., 2020), while many papers have shown this to be the case when aerosols exist over the boundary layer, although such has only been demonstrated in different parts of the world (C. Wang, 2013). The aerosols as produced in

Continental Southeast Asia have been demonstrated clearly, via direct lidar measurements as well as vertically resolved measurements of co-emitted species like CO, to be almost exclusively above the boundary layer in this part of the world during the local biomass burning season (Cohen et al., 2018; C. Lin, Cohen, Wang, & Lan, 2020; C. Lin, Cohen, Wang, Lan, et al., 2020; N.-H. Lin et al., 2013). For these reasons, the modeling work presented here also aims to explore the impact of such a large amount of aerosols above the boundary layer over this region of the world, and to understand what contribution if any to this unique event is being made through these dynamical/aerosol interactions.

This work establishes that in fact the enormous biomass burning events in Eastern India and Northern Southeast Asia are an important and significant source of pollution to the Maritime Continent and in specific the middle free troposphere (in contradiction to (Bianchi et al., 2020)). This new finding depends on larger emissions, an expanded emissions source area and complex 3-D transport mechanisms, and explains why such transport pathway has not been clearly established before. The resulting pathway of pollutants are demonstrated to be consistent with remotely sensed measurements in general and extreme events in particular. The observed and modeled loadings in theory should exhibit a significant forcing on the in-situ atmosphere, possibly linking the observed extreme heights to which the aerosols are observed to the complex terrain, unique and variable meteorology over these regions, and other factors which are not currently clearly understood, but are possibly linked to the effects of the aerosols themself.

2 Materials and Methods

2.1 AERONET Climatology

Aerosol Robotic Network AERONET (AERONET) project is a federation of ground-based remote sensing aerosol networks established by NASA (Holben et al., 1998), using upward-looking ground-based measurements of aerosol optical depth (AOD) at eight wavelengths (0.34, 0.38, 0.44, 0.50, 0.67, 0.87, 0.94 and 1.02um), as well as inversion products such as single scatter albedo (SSA) and column total water vapor (O'Neill et al., 2003; Schuster et al., 2005), at more than 430 sites worldwide. In this work we employ measurements of AOD and angstrom exponent as well as inverse AAOD product (when AOD>0.4 (Cohen & Wang, 2014)) using the all points Version 3 Level 2.0 data, from Jan 2010 to Dec 2018 at 10 sites located throughout Southeast Asia (Figure 1S). A few advantages of these measurements are that they function under very high values of AOD, they are more successful at filtering clouds from aerosols, they record multiple times a day, and finally that there are many more spectral channels available. All of this leads to lower error, improved reliability of the time variation of data at daily or even higher time scales, as well as higher precision and accuracy, as demonstrated in Southeast Asia by many previous studies (Cohen et al., 2018; S. Wang et al., 2020).

2.2 TRMM Multi-Satellite Precipitation Analysis (TMPA) Climatology

The Tropical Rainfall Measuring Mission (TRMM), an experimental satellite developed by The National Aeronautical and Space Administrations (NASA) of The United States and The National Space Development Agency (NASDA) of Japan, was launched in 1997 and closed in 2015. Following the shutdown of the TRMM satellite, the TRMM multi-satellite precipitation analysis (TMPA) database using the 3B42 algorithm continues to be called TRMM Version 7. It provides meteorologists with a large number of meteorological data such as tropical ocean

precipitation, liquid water content in clouds and latent heat release (Huffman, 1997; Huffman et al., 2007; Rosenfeld, 1999).

In specific, we employ daily TRMM measurements (Version7 Level 3) from 2010 to 2018 over Southeast Asia, at a resolution of 0.25^{o} X 0.25^{o}. Due to the precipitation is influenced by monsoon and local pollution levels, and meanwhile it could remove the aerosols that monsoons bring from upstream and usually lead to the end of the fire season, it's important to understand precipitation.

2.3 WRF-Chem Configuration

Weather Research and Forecasting model coupled with Chemistry (WRF-Chem) is a commonly used to compute meteorological (Fast et al., 2006; Grell et al., 2005) and the chemical transport equations of various tracers and chemical active species, at regional and meso scale (Girach et al., 2017; Kumar, Naja, Pfister, Barth, & Brasseur, 2012; Kumar, Naja, Pfister, Barth, Wiedinmyer, et al., 2012). This work used WRF-Chem version 3.6.1 to reproduce meteorology and atmospheric chemical composition over Southeast Asia including but not limited to turbulence, microphysical interactions, atmospheric chemical reactions, and aerosol processing. The meteorological fields were initialized using the National Centers for Environmental Prediction FiNaL reanalysis (NCEP-FNL) data, and the terrain data includes 24 land use categories from the U.S. geological survey. The chemical mechanism used is CBMZ, with the MOSIAC aerosol parameterization (Zaveri, Easter, & Peters, 2005; Zaveri, Easter, & Wexler, 2005), so as to include an intermediate number of gasses (55 gasses, 134 photolysis reactions), and externally mixed aerosols (including sulfate, nitrate, ammonium, sea salt, organic carbon, black carbon, and in-situ water), including size-resolved thermodynamic equilibrium, deposition, nucleation, and coagulation.

Southeast Asia is specifically defined in thus work as a mesh of 6.6km x 6.6km grids, 49 layers high, over 124 (east-west) by 149 (south-north) grids covering the regions from [-9.1, 26,3], [92.4, 122.6], with a maximum time-step of 2 minutes. The region was run from February 1st to March 31st 2016, so that the known observed biomass burning sources in Myanmar, Thailand, Laos, Cambodia, and Vietnam, as well as regions which thought to possibly be impacted by downwind transport, including Greater China, Southern Thailand, Malaysia, Singapore, and Indonesia are all included (Figure 1S).

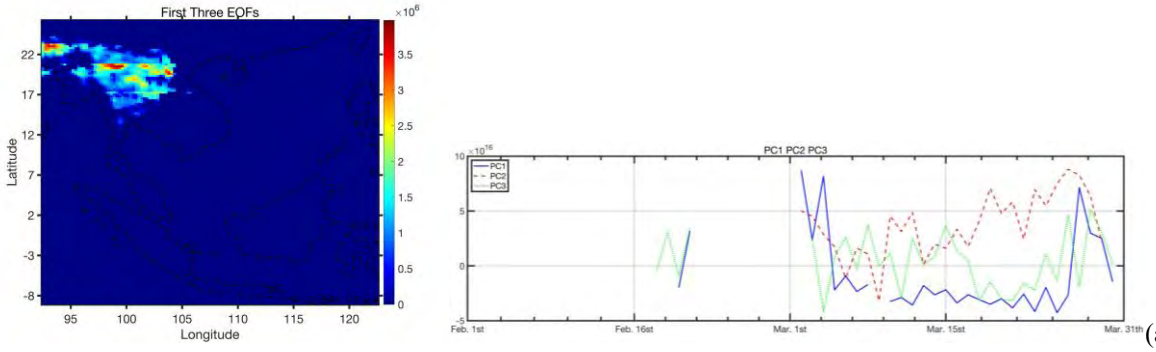

(a)

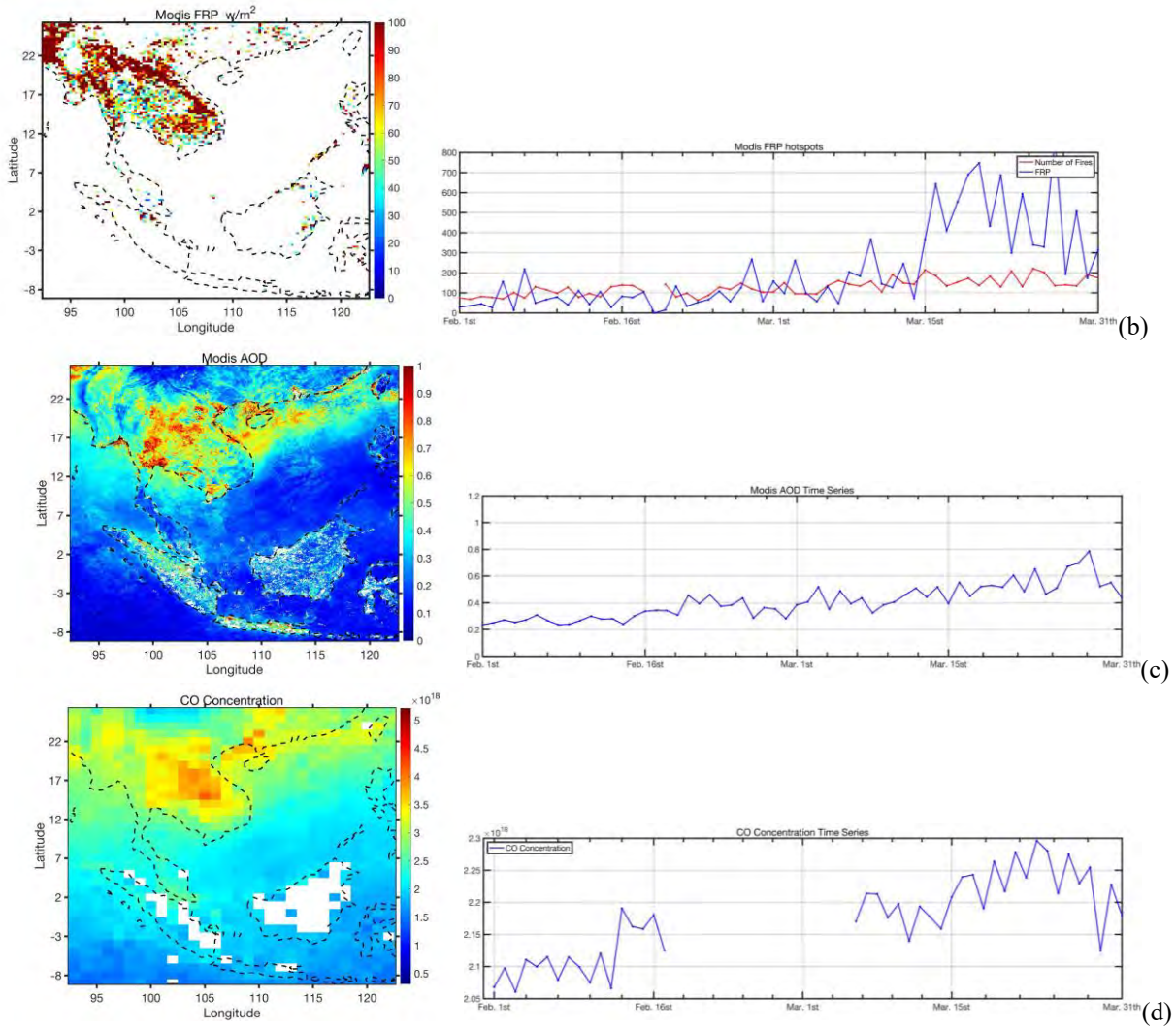

Figure 1. (a) Weighted sum of the first three EOFs (give in units of emissions - g/(km^2*h)) and the associated first three PCs, which control the daily timing of the emissions weight; (b) Distribution of hotspots from Modis instrument(give in units of power - w/m^2) and the associated time serials above 7^{o}N; (c) Distribution of AOD from Modis instrument and the associated time serials above 7^{o}N; (d) Distribution of CO from MOPPIT instrument (give in units of power - molecule/cm2) and the associated time serials above 7^{o}N.

2.4 New Daily, Chemically Consistent, Top-Down Emissions Inventory

This work uses a newly derived top-down emissions inventory computed using Empirical Orthogonal functions (EOFs) and Principle Components (PCs) in connection with daily remotely-sensed column measurements of NO_2 from the OMI satellite from 2016 over South Asia, Southeast Asia, and East Asia (Cohen, 2014; Cohen et al., 2017; C. Lin, Cohen, Wang, & Lan, 2020). The emissions are derived by selecting those spatially orthogonal maps which contribute at least 5% to the total variability, and using the associated temporal weighting of these maps to describe the constraints on the measured time series of NO_2 from OMI, following (C. Lin, Cohen, Wang, Lan, et al., 2020). The net produced NO_2 emissions have a 0.25^o X 0.25^o

spatial resolution and a daily temporal weighting. In this specific case, the resulting emissions depend on the weighted sum of the first 3 EOFs and the respective weighted first 3 PCs as given in (Figure 1). Biomass burning emissions of the other chemical species required to run WRF-Chem, specifically including NO, CO, OC, HCHO, etc. are all scaled respectively based on the ratios of the emissions factors of the species concerned and NO_2 as given by GFEDv4 (van der Werf et al., 2017). The only exception is that the emissions of BC are scaled so as to fall within the bounds provided by the global inversion of BC done by Cohen and Wang(Cohen & Wang, 2014). This provides a set of emissions which are smooth and consistent as much as possible with both the new top-down NO_2 spatial-temporal distribution, as well as other constraints from measurements where they exist.

2.5 Daily Measurements of AOD and Fire Hot Spots from MODIS and CO from MOPITT

Daily measurements of AOD at 3km resolution and FRP at 1km resolution were obtained from MODIS, and CO at 1^o resolution from MOPITT over the domain of this study. Since these are measurements of aerosols and CO co-emitted from the same biomass burning and urban sources analyzed in this work and presented in section 2.4, they offer an independent basis point by which to evaluate the goodness of the model results and scientific findings based on the new top-down NO_2 spatial-temporal distribution. Due to the fact that the total AOD and CO have different processes in-situ, these results provide support to whether or not the in-situ processing is also important. The mean daily values over the entire domain and their average time series computed between 7^oN and 25^oN from February 1st through March 31st for the three species are given in Figure 1 (B) (C) (D).

2.6 Daily Measurements of AOD and Fire Hot Spots from MODIS and CO from MOPITT

An explicit geospatial area [Tongue Region] unique to the high pollution days HSD and HDD is formed by comparing the difference of concentration of the single largest modeled component, BC4, between the high days and the climatology in Feb. and Mar. The BC4 is analyzed using two filters consistent with the tongue region both being polluted and having a change that is significant compared to the errors in the modeled fields and measurements. first, that the concentration on the high days is 25% larger than the climatology; and second that the ratio of the high days concentration to the climatology is at least a factor of 2.

3 Results

The new biomass burning emissions used in this work are found to occur throughout Eastern India, Myanmar, Northern Thailand, Laos, Cambodia, and Vietnam (Figure 1A) regions which tend to not have many densely populated urban areas and which have emissions dominated by fires (Figure 1B). Known urban areas in Northern Vietnam (co-located with the fires) and Southern Greater China, are found to be downwind (Figures 1C,1D). Additional high-density urban areas are also found in Central Thailand south or west respectively of the biomass burning regions, Southern Vietnam (co-located with the fires), and much further afield in Southern Thailand, Malaysia, Singapore, and Sumatra, more than 1000km to the South.

AERONET AOD measurements are analyzed to independently and objectively determine which periods are fire-influenced and which are not at locations far away from the fire source

region (Table 1, Figure 2). This data provides a climatology of AOD and strong variations from this climatology, as a function of space and time, allowing for abnormally high periods of AOD to be distinguished. TRMM data differentiates the regions based on climatological and day-to-day variation in rainfall, again allowing further analysis over a wide spatial scale of those regions influenced by rain or drought (Figure 3).

3.1 Properties of AERONET AOD

Ten sites from AERONET located in Southeast Asia were employed in this work to analyze the biomass burning season that occurred in 2016 (Figure 1S). Three of the sites (Chiang mai, Hanoi and Baclieu) are located in the biomass burning emissions source region, four of the sites (Hong Kong, Dongsha, Lulin, Taizhong) are located eastward from the biomass burning region, while the remaining three sites (Songkhla, Penang and Singapore) are located southward from the source region. Normally, during this season pollutants are transported from west to east with the shifting of the monsoon, with downwind transport taking a few days up to a week to appear in Guangdong and Hong Kong, Dongsha, and ultimately Taiwan.

In a typical year during February and March, there is heavy rain at Songkhla, Penang and Singapore, which typically are clean. However, in February and March of 2016 the three southern sites were found to have extremely high AOD 440nm measurements on six days, supporting the idea that these pollutants originated elsewhere and were advected to this region (Figure 2). A comparison against measurements during the annually recurring biomass burning time from February and March, as well as the overall climatology from 2010-2018 both reveal that 2016 was abnormal in this respect. As a result, the subset of data from March 13th to March 16th is hereafter labeled [HSD] and the subset of data from March 15th to 18th is subsequently labeled [HDD]. These specific cutoffs are chosen when there is a continuous surge of the AOD 440nm measurements over 0.4 for the entire period of interest at the entire group of source region sites and/or southern downwind region sites respectively.

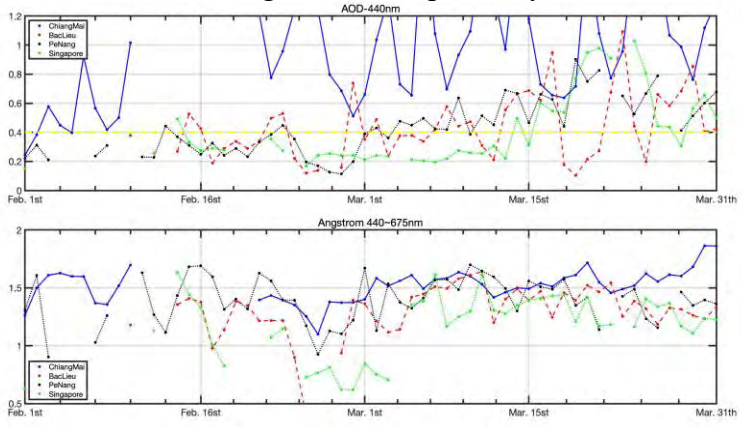

Figure 2. Time series of daily average measurements of AERONET AOD at 440nm and Angstrom coefficient from 440nm to 675nm

In Chiang Mai and Hanoi, the 2016 mean HSD AOD values are 1.14 and 1.56 respectively, an increase of 20% and 77% compared to the climatological biomass burning season. During the HSD time period in Chiang mai the AAOD was as high as 0.12, a 20% increase over the climatological value, while at the same time the Angstrom Exponent was about 1.5, indicating that the emitted BC was consistent with fresh and small particles (since there is

little to no dust in this region (Cohen & Wang, 2014), changes in the AAOD are highly representative of changes of the BC). In Hanoi, the Angstrom Exponent was found to be about 1.1, which is still representative of relatively small particles, but still particles which are far larger than the normal biomass burning time of 1.3 in this region. This set of results is consistent with Chiang Mai and Hanoi both being source regions, while Hanoi itself is also downwind with respect to particles exported from Chiang Mai and other far-upwind source regions, all mixed together with its otherwise typical urban signal. Overall, these results are consistent with the HSD time period in 2016 being an exceptionally large burning event.

Baclieu south of the west-to-east Chiang Mai to Hanoi advective route, although it is located upwind from the portion of the source region defined by the second EOF and PC. Although this region may be either dry or wet, with influence from both the north and the south, in 2016 during the HSD and the HDD the AOD is found to have values of 0.63 and 0.61, a respective increase of 47% and 42% over the typical biomass burning period. In terms of AAOD, the value is found to by 0.036 on HDD, a 24% increase in BC from a typical season. The Angstrom Exponent was found to be 1.44 and 1.39, which is a 11.6% and 7.8% decrease respectively, corresponding to a higher fraction of newer and hence smaller particles, consistent with a higher than normal fraction of fresh biomass burning emissions. Similar to Hanoi, there is a sizable amount of local urban emissions, but during the HSD and HDD times, this is not shown to be too significant. The fact that Baclieu registers as being uniquely elevated during both time periods indicates that it is not only a source region, but also potentially a pathway by which the northern biomass burning sources ultimately transported to the south.

Throughout the downwind regions, the magnitude of AOD reflects that the burning season of 2016 is atypical. The AOD at Dongsha is 0.28 higher compared with the general biomass burning climatology. HK, NCUEPA and Lulin are slightly lower in 2016 than the climatology, but this is not inconsistent, since on HSD and HDD days there was no data due to continuous cloud coverage. Secondly, the Angstrom Exponent measured at HongKong, Dongsha, and Lulin was smaller in 2016 compared to the other biomass burning years, indicating that the overall particles sizes were larger, consistent with a higher fraction of the total column aerosol being from ultra-long-range transport. Thirdly, the change of AAOD in the 2016 burning season seems to be only slightly lower in Dongsha and NCUEPA, while it is slightly higher in HK, even though the highest AAOD days at NCUEPA and HK had no measurements made due to cloud coverage. Similar patterns are observed in the AOD and MOPITT data further to the south over the South China Sea on these days, where there is no more large-scale cloud cover. These results are consistent with the fact that more aged aerosol will continue to acquire and/or grow a reflective/scattering shell around the BC core, leading to the aged aerosols possibly becoming less absorbing if the shell size grows too large (consistent with Cohen and Wang (Cohen & Wang, 2014) in this part of the world).

Although Singapore, Songkhla and Penang are normally rainy and hence have a very low AOD in February and March, in 2016 the AOD values of these three sites on HDD were 0.5, 0.51 and 0.55 respectively(Table 1), an increase of 0.06 to 0.12 compared to previous years, with the entirety of the difference occurring only over a small number of days. In addition, there is also a significant increase in the AAOD on the HDD days, from a climatological value of 0.012 to a 2016 value of 0.044. These findings are all consistent with the measurements observed during the HSDs from the source regions of Chiang Mai and Hanoi, both the HDD days and HSD in Baclieu, and the high HDD in Songkhla, Penang, and Singapore. This is a first piece of

evidence to support that in 2016 there was a significant amount of transport of biomass burning from as far north and west as Western India, Myanmar, Northern Thailand, and Laos to these equatorial destinations.

3.2 TRMM precipitation and WRF-Chem meteorology

Consistent changes are observed in the precipitation and meteorological measurements supporting the idea of ultra-long-range transport of aerosol particles during the HSD and HDD in 2016 as compared to the rest of 2016 and the biomass burning season climatology. First, the biomass burning season is always found to have less precipitation than the rest of the year north of 7oN, including both in the source regions and the typical downwind regions, stretching from Eastern India to the Western Pacific Ocean. In the biomass burning season, the rainfall in the south is mainly concentrated in the western and central parts of Indonesia, while the rainfall in the north, if any, is mainly concentrated in Southern Fujian and Taiwan (Figure 3).

In 2016 during the HSD and HDD days, most of the sites had an even lower amount of rainfall than typical this time of the year (Table 2). For example, the rainfall during the burning season in Hanoi and Baclieu in previous years was found to be an extremely dry 0.4mm, although the rainfall in 2016 was 0.13mm, and both the HSD and HDD days were 0.01mm respectively. This finding is consistent with 2016 having both an increase in biomass burning emissions, and reduced removal of articles, both leading to an enhanced atmospheric loading. The net effect in turn leads to larger scale aerosol cooling at the surface and more intense heating in the lower free troposphere, possibly further drying the land, promoting expansion of the biomass burning. This could also produce currents due to the heating in the lower free troposphere.

Different from other years, during 2016 the downwind areas in the east (including Guangdong, Hainan, northern South China Sea, Macau, Hong Kong, Fujian, and Taiwan) except for Dongsha (which was similarly drier than previous years) and NCU (which had slightly more rainfall than previous years) were all found to have more rainfall than normal. The specific difference between HSD, HDD and Climatology can be found in Figure 3(D, E, F), showing that there was a shift in the rainfall pattern this year to the south, with more rainfall over the Northern South China Sea and some parts of Fujian, while less fell inland. Further complicating this issue is that the overall wetter environment, seemingly shifted southward, was observed to be slightly smaller on HSD and smaller still on HDD days.

Furthermore, during the HSD and the HDD days, the overall precipitation from 5oN to about 1oS has been reduced enormously. Areas over land such as in southern Thailand, southern Vietnam, Malaysia, Singapore, the North Coast of Borneo, and the central and southern South China Sea were all found to be much drier than average. In particular, there was no rain recorded at the Songkhla, Penang, and Singapore AERONET sites throughout this period of time. Furthermore, there was a reduction of the normally heavy precipitation observed during the HDD throughout Sumatra, Malaysian Borneo, Western Indonesian Borneo and the region of the South China Sea in between these land areas.

In terms of meteorology, aerosols emitted from Eastern India, Myanmar, Northern Thailand, Laos and Northern Vietnam will have a high chance of being caught in the Southern Himalaya up-slope currents (Stone et al., 2010; Venzac et al., 2008) as well being co-emitted with buoyancy from biomass burning (Cohen et al., 2018; S. Wang et al., 2020). These two

effects lead to a significant amount of aerosols and trace gasses (C. Lin, Cohen, Wang, Lan, et al., 2020) being lofted high above the boundary layer over this region, from 850mb up to 650mb. In a normal year during February and March, due to change in the Monsoon's direction, the wind at this height flows from the west to the east, extending into the Pacific.

The climatology of the meteorological field on HSD and HDD (Figure 4), both show the wind divided by a line at about 12^{o}N, above which the wind blows from southwest to northeast, and below which the wind flows from northeast to southwest. The general climatology of the February and March wind fields from (from 700mb-950mb) show significant differences as a function of level and location. The wind fields in particular near the ground at 950mb and 900mb both show a very strong Northeast to Southwest wind extending from Southeastern Greater China to the Malay Peninsula and Sumatra, with almost no air flow over Thailand, Laos, and Northern Vietnam, and a strong Southwest to Northeast flow from Bangladesh and Myanmar through Yunnan. At 850mb to 800mb there is a strong break-point in the wind occurring as a continuous line from about 15^{o}N in the western portion of the domain studied to about 20^{o}N in the eastern portion of the domain studied. The wind blows strongly from the southwest to the northeast north of this line, and strongly from the northeast to the southwest south of this line. Climbing to 750mb to 700mb, this bifurcation in the wind field continues to move southward. Although still anchored at about 15^{o}N in the west, it has shifted down elsewhere and resides at around 17^{o}N in the east. There is another break point in the meteorology observed at about 2^{o}N found from 800mb and lower, which is consistent with the shift in the northward edge of the intense precipitation measured by TRMM over this region. What is interesting is that this gap does not extend east from Singapore at 750mb and seems to only exist over the Indian Ocean at 700mb.

During the special 6-day event examined in this work in 2016, the very high measurements of AOD seem to correspond to a southward perturbation in the atmosphere, as compared to what is typically observed (Figure S2). Based on the meteorology observed over the period, this finding is consistent with a source capable of first lofting the aerosols over the Central, Western South China Sea (from 20^{o}N to 17^{o}N) into the lower free troposphere (850mb to 700mb), followed by being caught in the strong Northeast to Southwest flow which then formed during the special days analyzed from the Central, Western South China Sea towards Southern Thailand and the Malay Peninsula. This is consistent with a source originating in the lower free troposphere over northern Continental Southeast Asia and transported to the east many days before, only to be re-directed to the Southwest during this special period of time.

These observed southward shift in the general precipitation pattern throughout this region from TRMM is consistent with the enhancement of the emissions due to the ultra-dry conditions over the source regions. This is supported by evidence in the precipitation and wind fields, which show a very clear Southward push in cold air leading to precipitation over Guangxi, Guangdong, Fujian, and Taiwan, as well as the Northern South China Sea, as well as the strong dry air advecting south over Southern Vietnam, Northern Thailand, Malaysia, Singapore, Sumatra and the Southern South China Sea down to the Borneo boarder. While these results do not attribute the shift in to the southwest that occurred during this time, the story is consistent with the idea that the extremely high loadings of BC generated and found over both the land and the South China Sea during this time having an impact on the meteorology itself, further reinforcing this southwestward flow, as observed by (C. Wang, 2013).

		Chiang Mai	Hanoi	Baclieu	Dong Sha	HK	NCUE PA	Lulin	Singapore	Songkhla	Penang
AOD	Climatology	0.55	0.83	0.32	0.39	0.55	0.49	0.71	0.48	0.29	0.39
	Burning Season Climatology	0.84	1.19	0.41	0.56	0.60	0.67	0.47	0.50	0.31	0.41
	2016 Burning Season	0.95	0.88	0.43	0.84	0.42	0.64	0.34	0.41	0.45	0.43
	High Source Days	1.14	1.56	0.63	NaN	NaN	NaN	NaN	0.41	0.45	0.62
	High Destination Days	0.80	NaN	0.61	NaN	NaN	NaN	NaN	0.50	0.51	0.55
Angstrom	Climatology	1.43	1.29	1.15	1.18	1.31	NaN	1.25	1.40	1.16	1.33
	Burning Season Climatology	1.58	1.28	1.21	1.27	1.28	NaN	1.30	1.28	1.20	1.36
	2016 Burning Season	1.51	1.31	1.29	1.22	1.21	NaN	1.19	1.17	1.37	1.39
	High Source Days	1.50	1.12	1.44	NaN	NaN	NaN	NaN	1.36	1.59	1.47
	High Destination Days	1.53	NaN	1.39	NaN	NaN	NaN	NaN	1.42	1.48	1.53
AAOD	Climatology	0.105	0.067	0.037	0.032	0.046	0.038	0.032	0.028	0.039	0.036
	Burning Season Climatology	0.135	0.111	0.040	0.043	0.038	0.045	0.033	0.020	0.050	0.038
	2016 Burning Season	0.101	0.148	0.029	0.033	0.041	0.044	NaN	0.009	0.045	0.042
	High Source Days	0.120	NaN	0.025	NaN	NaN	NaN	NaN	0.006	0.043	0.034
	High Destination Days	0.089	NaN	0.036	NaN	NaN	NaN	NaN	0.012	0.046	0.044

Table 1. Statistics of daily AERONET version 3 level 2.0 measurements of AOD at 440nm and Angstrom coefficient from 440nm to 675nm over the polluted regions

	Climatology	Burning Season Climatology	2016 Burning Season	High Source Days	High Destination Days
Overall	6.52	4.13	4.32	3.75	3.28
North	5.63	1.46	1.11	0.97	0.68
South	7.58	7.25	8.05	6.98	6.31
Chiang Mai	3.53	0.45	0.13	0.00	0.00
Hanoi	4.85	0.37	0.01	0.00	0.00
Bac lieu	5.13	0.48	0.01	0.00	0.00
Dong Sha	5.19	2.07	2.84	7.13	1.69
HK	4.31	1.79	2.44	0.00	0.00
NCUEPA	4.27	2.88	5.28	26.83	7.29
Lulin	5.86	1.32	2.06	9.37	0.00
Singapore	6.24	4.91	4.17	0.00	0.00
Songkhla	6.22	2.05	0.26	0.00	0.00
Penang	7.34	5.11	1.13	0.00	0.00

Table 2. TRMM precipitation data from Jan. 2010 to Dec. 2018, with the north/south regions separated at 7^{o}N

3.3 Spatio-temporal variation of BC concentration modeled with WRF-Chem

In order to verify the hypothesis, an improved emission inventory was formed based on the first three principal components of the EOF of the daily OMI remotely sensed NO_2 column loading. Both this measurement constrained emissions inventory [EOF-Emissions] of the extreme biomass burning events as well as the standard FINN-based hotspot emissions biomass burning inventory [Basic-Emissions] were used to drive WRF-Chem, and verify the possible transportation pathways of these extreme events. The focus of this modeling study is with respect to BC, since it is directly co-emitted with the NO_2 from the biomass burning events, has a relatively long chemical lifetime, has a relatively long deposition lifetime under the dry conditions found over most of the region during this special event, and is rapidly removed due to precipitation, as demonstrated previously (Cohen, 2014; Cohen et al., 2018; Cohen & Wang, 2014).

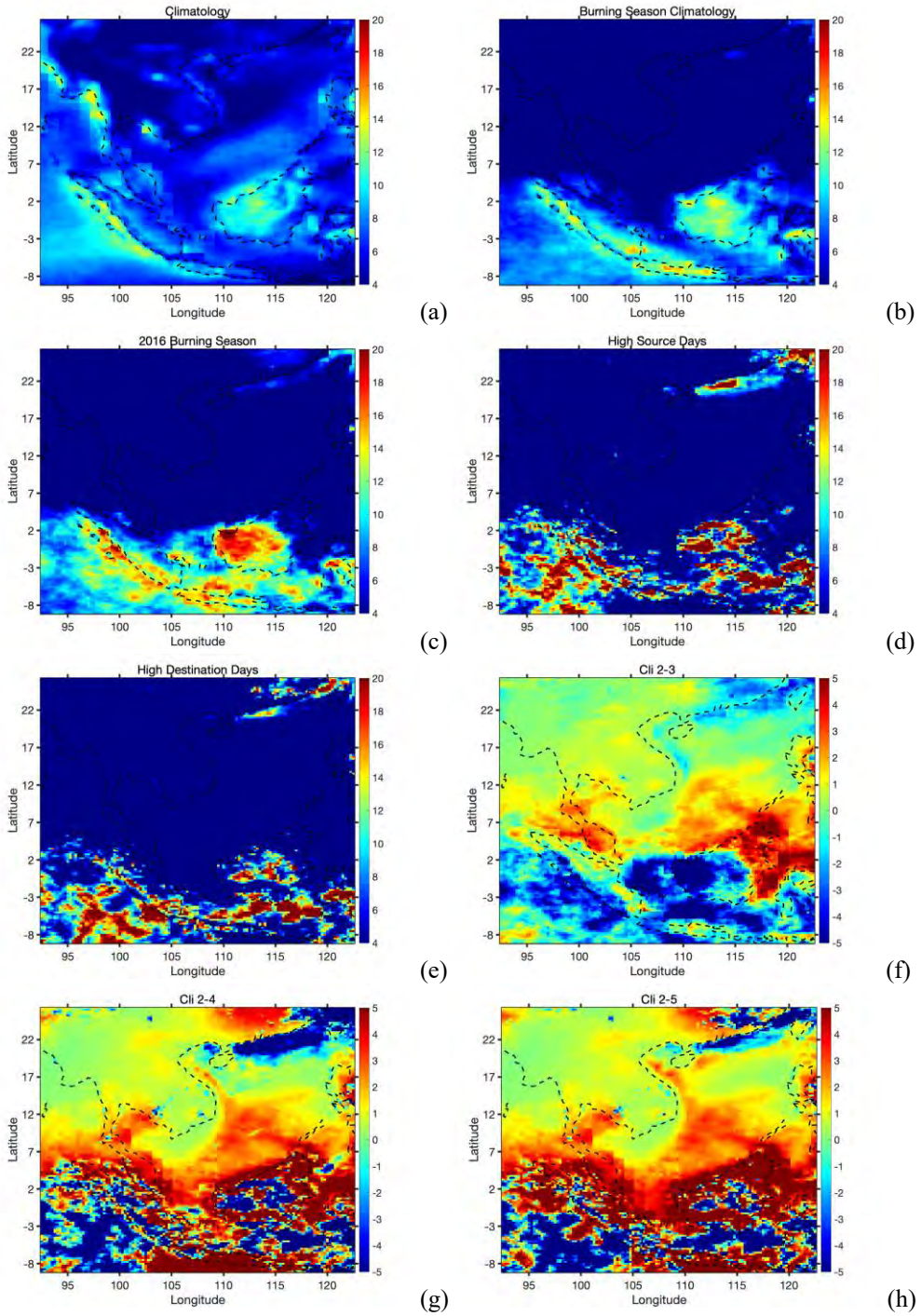

Figure 3. TRMM Climatology over the following times: (a) all months from 2010 through 2018, (b) all February and March days from 2010 through 2018, (c) all days February and March days in 2016, (d) high source days only, (e) high destination days only, (b) – (c), (b) – (d), (b) – (e))

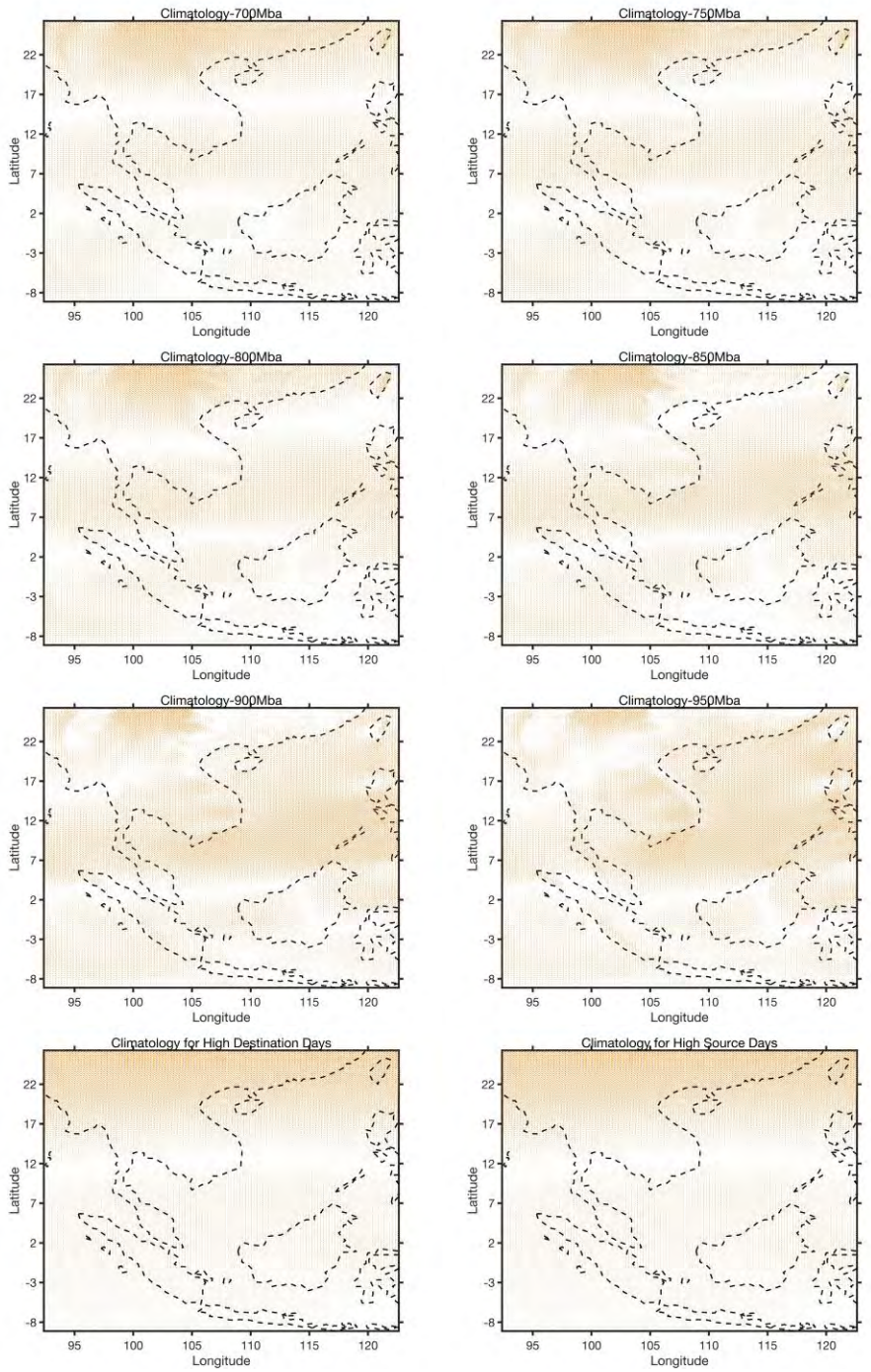

Figure 4. Climatological winds for all days in February and March 2016 given at different heights from 950mb up to 700mb

Within BC is tracked over 6 size bins in WRF-Chem and determined by mass to mostly be in size bins 3 to 6 (corresponding 156.3-312.5nm, 312.5-625nm, 625-1250nm, and 1250-2500nm) hereafter referred to BC3, BC4, BC5 and BC6 respectively. Due to the long time required to transport over such distances, the BC is expected to undergo depositional growth due to co-emitted semi-volatile species as well as NO_2 and SO_2 oxidized in the atmosphere in-situ (Jimenez et al., 2009; Singh et al., 2018). Therefore, a consistent story is obtained by showing

clearly that smaller sized particles dominate near the sources and grow as they travel downwind. Furthermore, at the concentrations observed, the absorption of a significant amount of solar radiation should occur, making a significant contribution to the in-situ heating of the atmosphere and henceforth on the energy balance and dynamics of the atmosphere over this region (Cohen et al., 2017; C. Wang, 2007).

The differences in the BC concentration loadings between the overall BC climatology from February 1st through March 31st is given in Figure 5. First, it is observed that the Basic-Emissions case does not yield long-range transport of BC over most of the South China Sea, only advecting as far as Vietnam, the Beibu Gulf and Hainan. Second, it is observed that the Basic-Emissions cases do not yield long-range transport south of 12oN. Third, the column loading of BC3, BC4, BC5, and BC6 in the Basic-Emissions case are a factor of a minimum of 6.6 (BC3) to a maximum of 11.9 (BC4) smaller than in the EOF-Emissions case over the [maximum region] (defined from 12oN to 26.3oN and 92.4 oE to 122.6oE) (Figure S4 and Figure S5).

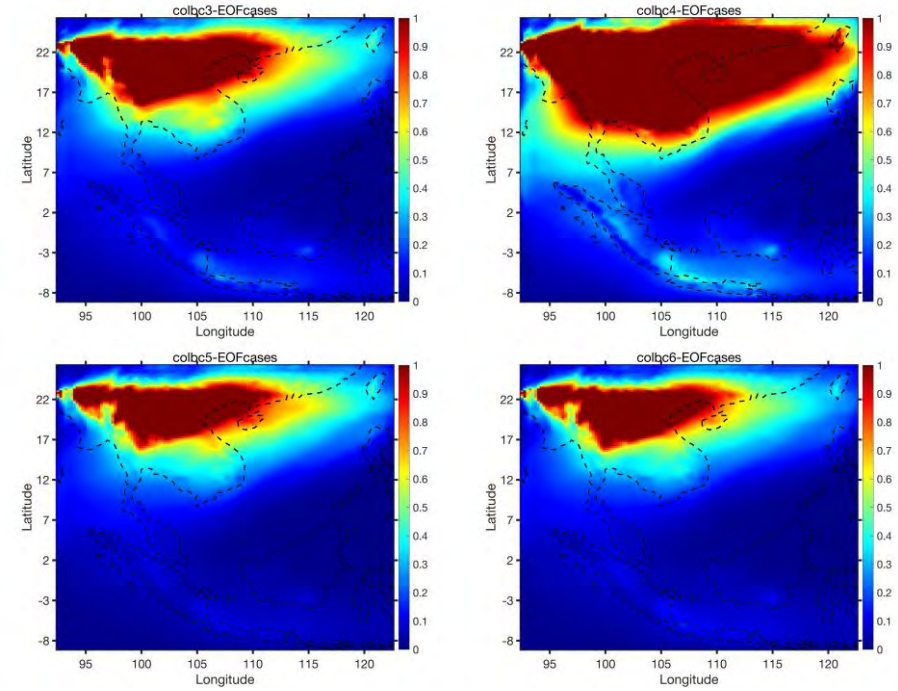

Figure 5. Climatology of total column BC concentrations over sizes 3 to 6 over all days using the EOF emissions

The climatology of the EOF-emissions case shows that the amount of BC mass ranges from least to most in size 3, 5, 6, and 4, with a climatological mean weighted concentration over the [maximum region] from 950mb to 700mb ranging from 0.66 ng/g (BC3) to 1.5 ng/g (BC4) (Figure S4, FigureS5). The spatial distribution shows the highest levels of BC over the biomass burning source regions in the north, with a smaller but still significant burden over emissions regions in the south. Second, there is a significant amount of eastward transport observed at all size ranges of BC, with the smaller sizes (BC1 and BC2) having a significant amount of transport two-thirds of the way across the South China Sea (to about Dongsha Island) and the larger size ranges (BC3 to BC6) exhibiting eastward transport all the way to Taiwan or beyond into the Pacific Ocean, consistent with the flow induced by the Indian Ocean monsoon on observations of CO (C. Lin, Cohen, Wang, Lan, et al., 2020). Third the geographic spread of

BC4 has the largest total area, reaching as far east as the Western Pacific Ocean, as far South as 7°N, as far southeast as the Philippines, and as far southwest as the Indian Ocean. Similarly, the spread of BC5 and BC6 is similar east-west to BC3, but slightly stronger north-south more similar to BC4, consistent with the transport pathway to the south only occurring for more aged particles.

The specific spatial distribution of the BC is significantly different from the climatology on the six HSD and HDD days (Figure 6), especially so for BC3 to BC6. First, there is a significant amount of additional BC transported to the East, from as far north as the East China Sea, to as far south as Minando. Secondly, there is a significant loading flowing Southwest reaching through the Gulf of Thailand, the Southern South China Sea, the Malay Peninsula and Singapore, to Sumatra. Overall, there is a significant amount of black carbon particles that have moved thousands of kilometers away from the source region, with the vast majority found over the China South Sea and with such a magnitude that it contributes significantly to the AOD even in urban areas far downwind, as observed in Guangdong, Fujian, Taiwan and the Northern reaches of the South China Sea. The heating generated by such a significant spread and concentration of BC will likely modify the West to East flow associated with the Indian Monsoon, pushing it further to the South, consistent with the southward shift of precipitation from 3°N to 5°N to 2°N to 3°S as observed during these high pollution days. Similarly, in the Southeastern parts of the South China Sea, the precipitation line and the BC concentration line have also both been observed to shift Southward from 7°N to 2°S. Finally, the high modeled loadings of BC3 and BC4 are consistent with the observations of AAOD and Angstrom Exponent from medium sized particles observed at AERONET stations in Southern Thailand, Malaysia, and Singapore during this time.

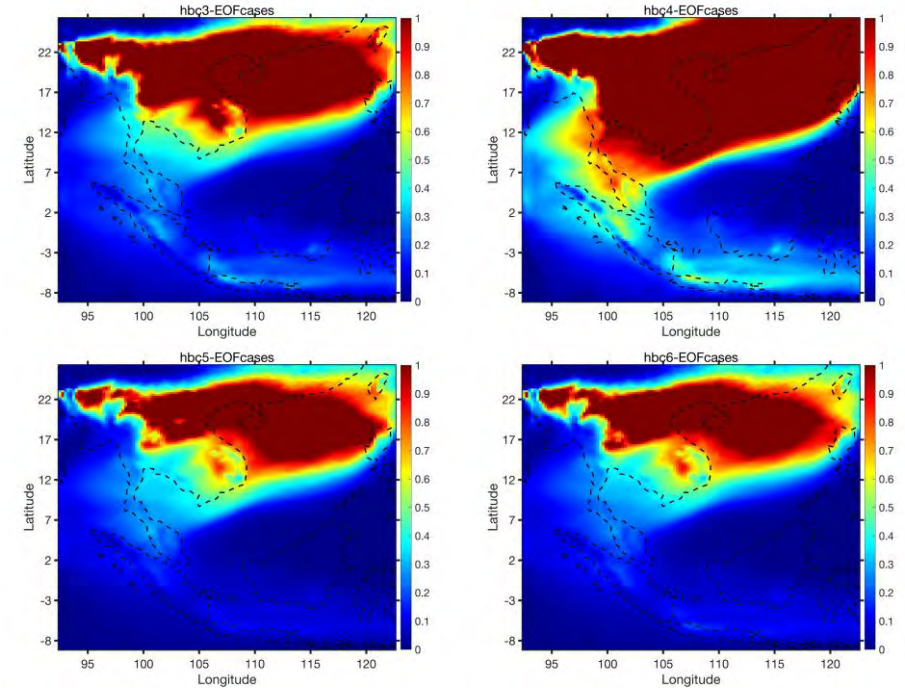

Figure 6. Climatology of column BC concentration for sizes 3 to 6 over the high pollution days using the EOF emissions

In general, the flow is found to occur from the west to the east throughout the highly polluted period, with the source region focused on the southern side of the Himalayas from Eastern India through Northern Vietnam. The outward flow generally stops at the Beibu gulf or Hainan island at 950mb, flowing through Dongsha Island at 900mb, and flowing all the way across Taiwan into the western Pacific from 850mb through 700mb. There is not found to be significant North to South flow on the first day, except for a small amount of flow from 850mb to 750mb over the western part of the South China Sea, and only as far south as the tip of Vietnam. On the second and third days, there is a detachment of the flow, with a significant amount of the East-West flow either continuing towards the east if it is north of 17^{o}N or redirecting towards the South and Southwest if it is south of 17^{o}N. This pattern is found to be especially true from 850mb through 750mb. It is observed that there is some downwelling south of 17^{o}N from the Southward and Southwestward branch, ultimately mixing back into the levels from 950mb to 900mb. At 700mb and above during this time, there is only a continuation of the west to east pattern, except for right along the coast of Vietnam. On the fourth day there is a

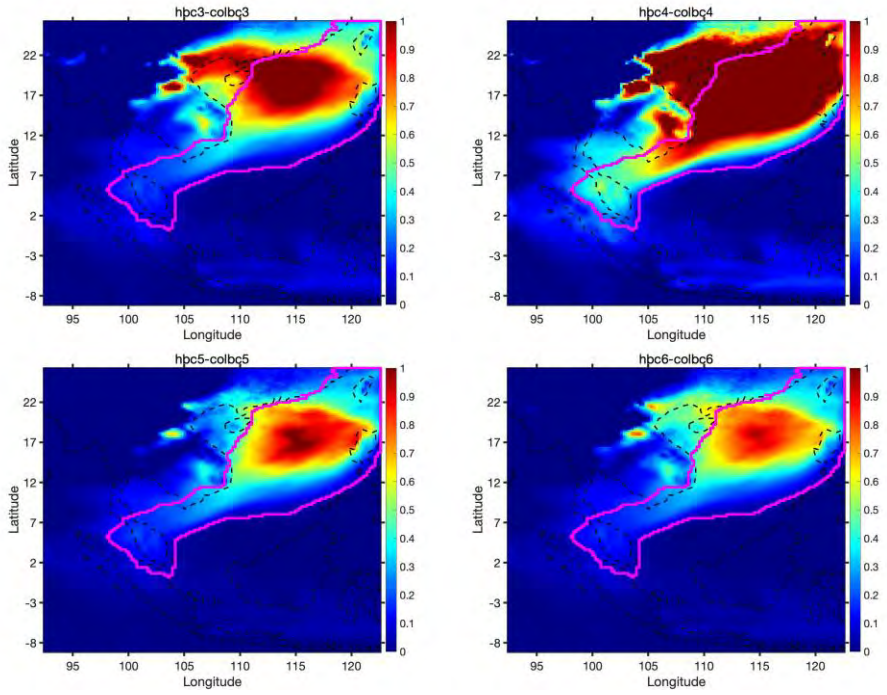

Figure 7. The difference in BC concentration for sizes 3 to 6 between the high pollution days and all days in February and March, as well as the definition of the tongue region, driven by EOF emissions

considerable southwestward flow from 900mb through 800mb, while at the same time there appears to be a downward mixing and flow allowing the material to mix down to 900mb, and causing the 750mb level and above to shift back into a West to East flow. On the fifth day, this continues, with there being strong flow to the Southwest from 850mb to 950mb, more downward flow and mixing the further south the particles travel, with the remaining particles at 800mb and above now switching back into a more typical West to East flow. On the final day the southwestward flow seems to weaken and the remaining aerosols that have been advected into

the region slow down, leading to stagnation and some dilution into the Eastern Indian Ocean and over Northern and Central Sumatra. With the flow now shut down, the aerosols here are slowly removed over the next few days due to dry deposition and the short-scale but intense localized convection found throughout the region.

This resulting flow is consistent with the timing and magnitude of the AERONET measurements in Southern Thailand, Malaysia, and Singapore. Consistently across these results, the aerosol transported far to the South seems to have a maximum to minimum concentration range of BC4, BC3, BC5, and BC6. Given that there are no emissions of BC in any size range larger than BC3, this is consistent with a significant amount of growth of the BC in-situ over a period of many days.

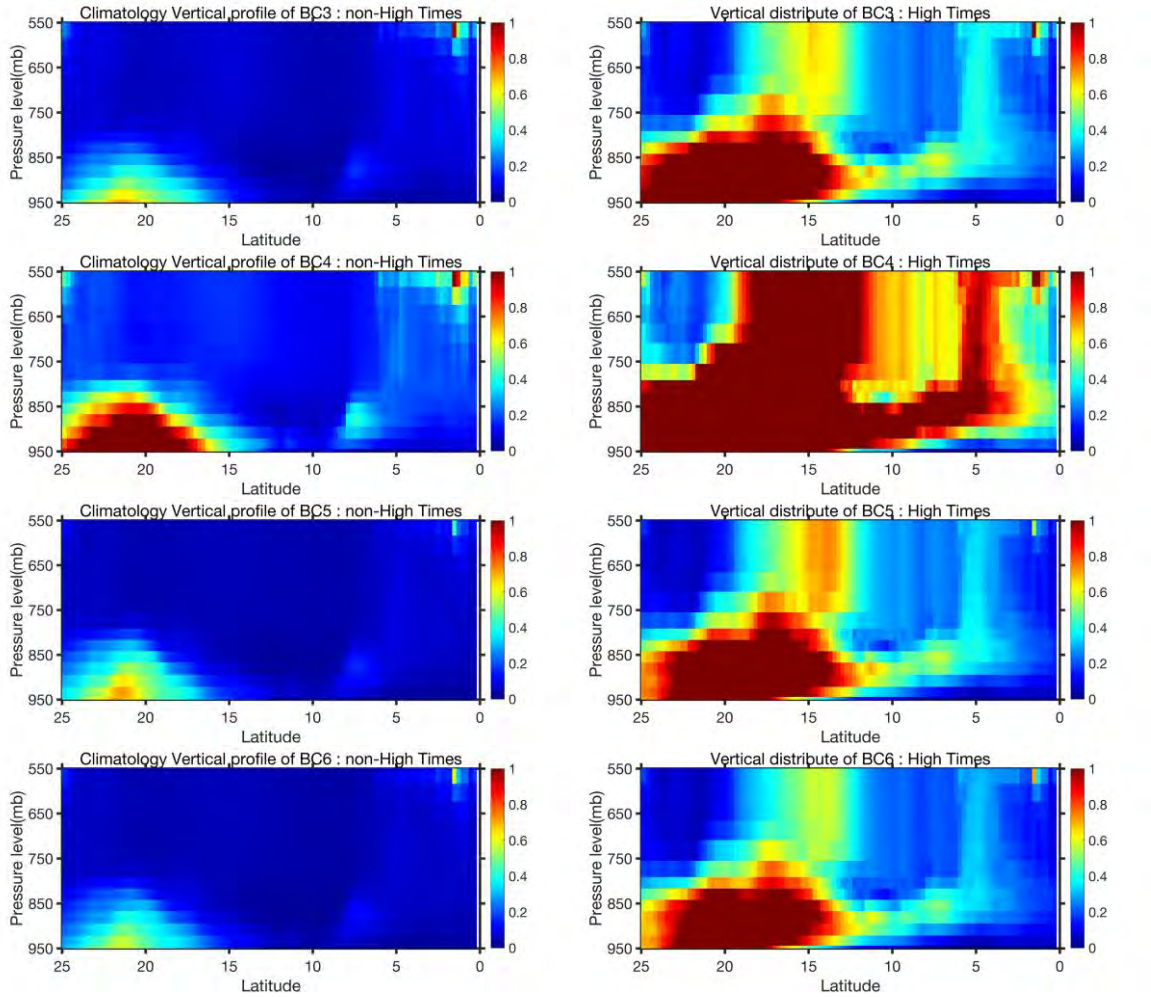

Figure 8. Vertical distribution of BC concentrations latitudinally averaged over the tongue region for sizes 3 to 6 for both all days (left) and high pollution times only (right) for the EOF emissions case

The region of maximal concentration on the HSD and HDD days [tongue region] (Figure 7, pink outline) is found to extend from Taiwan to Singapore during the high pollution days, with the largest differences observed over the Central parts of the South China Sea, Hainan, Cambodia, Southern Vietnam, Southern Thailand, Malaysia and Singapore. Given that most of

the regions within the tongue region are generally found to be clean, the observed loadings and any subsequent radiative effects are both significant. The latitudinal mean over each model grid in a west-to-east manner across the tongue region as a function of the height of the modeled BC (Figure 8) demonstrates that the vertical climatological distribution of the BC over the Tongue region (i.e. not during the six highly polluted days) is mostly confined between 25^{o}N and 15^{o}N, and from the surface through about 850mb. However, on the high pollution days, there is a vastly different spatial structure, with BC3 expanding from 12^{o}N to 25^{o}N from the surface up through a top of 750mb to 650mb, with the loadings above the level rapidly removed by deep convection. Furthermore, BC3 is found to have a significant southward branch occurring from 950mb through 750mb down to 5^{o}N, from which some of it diffuses all the way to the equator, some of its ages and grows into BC4 and some is removed due to deep convection and wet deposition. BC4 experiences a pattern similar to BC3 the notable differences being a slightly higher loading up to 800mb in the climatology, slightly more Equatorial flow during the extreme days, and a higher concentration almost everywhere not near the surface. BC5 and BC6 are more similar to BC4, with the exception that their concentrations are lower everywhere, due to the fact that there is insufficient time for significant growth into these even larger sizes.

5 Conclusions

This work quantifies the impact of a new top-down emissions inventory constrained by NO_2 column measurements of biomass burning from Eastern India through Northern Vietnam in February and March 2016 on the spatial and vertical distribution of black carbon particles and their subsequent long-range transport. Since the emissions used are based on NO_2, therefore the only connection between the measured and modeled aerosols and the emissions occurs at the place and time where the aerosols and NO_2 are co-emitted (including any rapid spread in the vertical). This approach uses definitive concentrations in the air, as compared with indirect measurements of FRP which may be masked or otherwise not related to emissions in the case of peat or wet ground. This approach also goes above and beyond the more standard approach of merely scaling known spatial and temporal distributions of fire emissions, which as demonstrated due to the fact that there are previously unidentified source regions, cannot reproduce the findings observed here.

There is a further emphasis on a six-day extreme pollution incident that occurred from March 13th to March 18th 2016, extending from the Southern foothills of the Himalayas all the way to the Western Pacific Ocean to the east and Sumatra to the South. While climatologically there are annually occurring biomass burning events from Eastern India through northern Vietnam as observed in this work as well as recently by MOPITT in other work, none of these have been incorporated into the current generation of fire emissions inventories. This years event was shown to be even larger in spatial and temporal scope, reaching into regions usually inundated by Monsoon rains at this time in Southern Thailand, Malaysia, Singapore and Sumatra. This approach shows clearly that the only way to match the measured extreme loadings of mid-tropospheric aerosols, CO, precipitation, and wind, is to use the new satellite-constrained top-down emissions dataset based on variance-maximization of NO_2 columns in combination with the 3-D transport and chemical growth and in-situ processing as modeled in WRF-CHEM.

The specific differences underling this finding are first that the region from Eastern India through Northern Vietnam has a large amount of lofted aerosols from a combination of heat from newly identified burning sources and upslope winds. These are subsequently transported from

west to east while continue to undergo growth and in-situ processing with a significant amount of BC aerosol advected to Hainan (BC2), Dongsha (BC3) and as far as Taiwan Island and the Western Pacific (BC4 and BC5), as well as further North and further South from (25^{o}N to 12^{o}N). This specific pattern is observed in the free troposphere, with aerosols found relatively consistently from 850mb up through 750mb, and as high as 650mb over a sizable part of the region. Secondly, during the high pollution days, there is a tongue shaped region which constrains a large branch of aerosols advected to the south and southwest, as far south as 2^{o}N-3^{o}S, as measured in Southern Thailand, Malaysia, Singapore, and Sumatra, a finding which is unprecedented this time of year due to typical Monsoon Rains extending to 5^{o}N-2^{o}S. Over this tongue shaped region, the particles were found to transport mostly initially from 700mb to 750mb (from 15^{o}N to 10^{o}N), from 800mb to 850mb from (12^{o}N to 2^{o}N, and from 900mb to 950mb from 10^{o}N to 2^{o}S), with diffusion and small-scale convection mixing the aerosols downward as they transport southward, and large-scale deep convection providing removal from the top layers via uplift and subsequent wet deposition. The induced atmospheric heating induced by such a substantial amount of BC aerosol, and reconfirmed by AAOD measurements from AERONET is consistent with a plume capable of self-stabilization and moderate convective suppression, consistent with both the results obtained and theory.

The new emissions lead to a source region having a large source spread over the geographic regions south of the Himalayas, which are ultimately advected upwards and into the correct place and at the correct height over the South China Sea to be able to get caught into the southward and southwestward advection regime and ultimately be transported to the equator. In most emissions databases, there are not enough emissions from this northern region, while those in the southern region do not have access to mountains to induce additional lofting. Furthermore, the higher amount of emitted NO_2 indicates more co-emitted heat and therefore buoyancy. Hence the combination of being in the proper place, at the right time, combined with a sufficiently large source strength are all required to enter into the Southward and Southwestern flow. Furthermore, since the BC in the Basic-emissions case is not in the free troposphere, subsequent radiative stabilization does not occur to keep the aerosols in-situe for a long enough time.

Given the extremely high loadings of aerosols found within urban areas in Southeast Asia during these extreme events, which otherwise should be clean due to heavy rain, this paper helps provide context into better understanding the causes and magnitudes of the contributions to such special events. Furthermore, it provides a consistent and hereas new pathway through which the aeorsols enter the free troposphere in Monsoon Asia. It is hoped that these new approaches can provide useful information for understanding health and climate impacts as well as a path towards towards mitigation for these rapidly developing regions of the world. Obvious challenges remain to expand the number of available emissions species, to incorporate more measurements, to expand these results beyond this year and this geographic region, and to better account for uncertainties in the measurements and the models. However, it is hoped that this work can help demonstrate clearly the need to take these steps and provide a roadmap for the community to move to the next level of biomass burning emissions and long-range transport studies and analyses.

Author Contributions

Shuo Wang: data curation, formal analysis, investigation, software, visualization, writing – original draft.
Jason Blake Cohen: conceptualization, funding acquisition, investigation, methodology, project administration, resources, supervision, validation, writing – original draft, review & editing.
Weizhi Deng: Partial code, digitizing, visualization.
Kai Qin: review.
Jianping Guo: review.

Code/Data availability:

All processed data, results, and codes are freely available for download at https://doi.org/10.6084/m9.figshare.13140047.v1

Conflict of Interest:

The authors declare that they have no conflict of interest.

Acknowledgements:

We would like to acknowledge the PIs of the AERONET, TRMM, GFED, OMI, MOPITT and MODIS instruments for providing the remote sensing measurements, and NCEP FNL reanalysis project for providing the meteorology measurements. AERONET measurements data could be downloaded from https://aeronet.gsfc.nasa.gov/cgi-bin/draw_map_display_inv_v3, TRMM multi-satellite precipitation analyses was obtained from https://disc.gsfc.nasa.gov/datasets/TRMM_3B42_Daily_7/summary?keywords=3B42, GFED data was obtained from https://www.geo.vu.nl/~gwerf/GFED/GFED4/, the meteorological fields of NCEP FNL data could be obtained from https://rda.ucar.edu/datasets/ds083.2/, OMI data could be obtained from https://disc.gsfc.nasa.gov/mirador-guide?tree=project&project=OMI, MOITT data could be obtained from https://eosweb.larc.nasa.gov/datapool, and MODIS data could be obtained from https://ladsweb.modaps.eosdis.nasa.gov/archive/allData/61/MOD021KM/2016/ and https://ladsweb.modaps.eosdis.nasa.gov/archive/allData/61/MOD04_3K/2016/. The work was supported by the Chinese National Young Thousand Talents Program (Project 41180002), the Chinese National Natural Science Foundation (Project 41030028; Project 42075147(accepted, number not yet available)), and the Guangdong Provincial Young Talent Support Fund (Project 42150003).

References

Abba, E. J., Unnikrishnan, S., Kumar, R., Yeole, B., & Chowdhury, Z. (2012). Fine aerosol and PAH carcinogenicity estimation in outdoor environment of Mumbai City, India. *International Journal of Environmental Health Research, 22*(2), 134-149. https://doi.org/10.1080/09603123.2011.613112

Aouizerats, B., van der Werf, G. R., Balasubramanian, R., & Betha, R. (2015). Importance of transboundary transport of biomass burning emissions to regional air quality in Southeast Asia during a high fire event. *Atmos. Chem. Phys., 15*(1), 363-373. https://acp.copernicus.org/articles/15/363/2015/

As-syakur, A. R., Adnyana, I. W. S., Mahendra, M. S., Arthana, I. W., Merit, I. N., Kasa, I. W., et al. (2014). Observation of spatial patterns on the rainfall response to ENSO and IOD over Indonesia using TRMM Multisatellite Precipitation Analysis (TMPA). *International Journal of Climatology, 34*(15), 3825-3839. https://rmets.onlinelibrary.wiley.com/doi/abs/10.1002/joc.3939

Bianchi, F., Junninen, H., Bigi, A., Sinclair, V. A., Dada, L., Hoyle, C. R., et al. (2020). Biogenic particles formed in the Himalaya as an important source of free tropospheric aerosols. *Nature Geoscience*. https://doi.org/10.1038/s41561-020-00661-5

Chang, C.-P., Wang, Z., McBride, J., & Liu, C.-H. (2005). Annual Cycle of Southeast Asia—Maritime Continent Rainfall and the Asymmetric Monsoon Transition. *Journal of Climate, 18*(2), 287-301. https://doi.org/10.1175/JCLI-3257.1

Chapman, E. G., Gustafson Jr, W. I., Easter, R. C., Barnard, J. C., Ghan, S. J., Pekour, M. S., & Fast, J. D. (2009). Coupling aerosol-cloud-radiative processes in the WRF-Chem model: Investigating the radiative impact of elevated point sources. *Atmos. Chem. Phys., 9*(3), 945-964. https://acp.copernicus.org/articles/9/945/2009/

Chen, J., Li, Z., Lv, M., Wang, Y., Wang, W., Zhang, Y., et al. (2019). Aerosol hygroscopic growth, contributing factors, and impact on haze events in a severely polluted region in northern China. *Atmos. Chem. Phys., 19*(2), 1327-1342. https://acp.copernicus.org/articles/19/1327/2019/

Chung, S. H., & Seinfeld, J. H. (2002). Global distribution and climate forcing of carbonaceous aerosols. *Journal of Geophysical Research: Atmospheres, 107*(D19), AAC 14-11-AAC 14-33. https://agupubs.onlinelibrary.wiley.com/doi/abs/10.1029/2001JD001397

Cohen, J. B. (2014). Quantifying the occurrence and magnitude of the Southeast Asian fire climatology. *Environmental Research Letters, 9*(11), 114018. http://dx.doi.org/10.1088/1748-9326/9/11/114018

Cohen, J. B., Lecoeur, E., & Hui Loong Ng, D. (2017). Decadal-scale relationship between measurements of aerosols, land-use change, and fire over Southeast Asia. *Atmos. Chem. Phys., 17*(1), 721-743. https://acp.copernicus.org/articles/17/721/2017/

Cohen, J. B., Ng, D. H. L., Lim, A. W. L., & Chua, X. R. (2018). Vertical distribution of aerosols over the Maritime Continent during El Niño. *Atmos. Chem. Phys., 18*(10), 7095-7108. https://acp.copernicus.org/articles/18/7095/2018/

Cohen, J. B., Prinn, R. G., & Wang, C. (2011). The impact of detailed urban-scale processing on the composition, distribution, and radiative forcing of anthropogenic aerosols. *Geophysical Research Letters, 38*(10). https://agupubs.onlinelibrary.wiley.com/doi/abs/10.1029/2011GL047417

Cohen, J. B., & Wang, C. (2014). Estimating global black carbon emissions using a top-down Kalman Filter approach. *Journal of Geophysical Research: Atmospheres, 119*(1), 307-323. https://agupubs.onlinelibrary.wiley.com/doi/abs/10.1002/2013JD019912

Deng, W., Cohen, J. B., Wang, S., & Lin, C. (2020). Improving the Understanding between Climate Variability and Observed Extremes of Global NO_2 Over the Past 15 Years. *under review*.

Ding, A., Wang, T., & Fu, C. (2013). Transport characteristics and origins of carbon monoxide and ozone in Hong Kong, South China. *Journal of Geophysical Research: Atmospheres, 118*(16), 9475-9488. https://agupubs.onlinelibrary.wiley.com/doi/abs/10.1002/jgrd.50714

Fast, J. D., Gustafson Jr, W. I., Easter, R. C., Zaveri, R. A., Barnard, J. C., Chapman, E. G., et al. (2006). Evolution of ozone, particulates, and aerosol direct radiative forcing in the vicinity of Houston using a fully coupled meteorology-chemistry-aerosol model. *Journal of Geophysical Research: Atmospheres, 111*(D21). https://doi.org/10.1029/2005JD006721

Field, R. D., van der Werf, G. R., & Shen, S. S. P. (2009). Human amplification of drought-induced biomass burning in Indonesia since 1960. *Nature Geoscience, 2*(3), 185-188. https://doi.org/10.1038/ngeo443

Forkel, R., Werhahn, J., Hansen, A. B., McKeen, S., Peckham, S., Grell, G., & Suppan, P. (2012). Effect of aerosol-radiation feedback on regional air quality – A case study with WRF/Chem. *Atmospheric Environment, 53*, 202-211. http://www.sciencedirect.com/science/article/pii/S1352231011010545

Girach, I. A., Ojha, N., Nair, P. R., Pozzer, A., Tiwari, Y. K., Kumar, K. R., & Lelieveld, J. (2017). Variations in O3, CO, and CH4 over the Bay of Bengal during the summer monsoon season: shipborne measurements and model simulations. *Atmos. Chem. Phys., 17*(1), 257-275. https://acp.copernicus.org/articles/17/257/2017/

Gonzalez-Alonso, L., Val Martin, M., & Kahn, R. A. (2019). Biomass-burning smoke heights over the Amazon observed from space. *Atmos. Chem. Phys., 19*(3), 1685-1702. https://acp.copernicus.org/articles/19/1685/2019/

Grandey, B. S., & Wang, C. (2019). Background Conditions Influence the Estimated Cloud Radiative Effects of Anthropogenic Aerosol Emissions From Different Source Regions. *Journal of Geophysical Research: Atmospheres, 124*(4), 2276-2295. https://agupubs.onlinelibrary.wiley.com/doi/abs/10.1029/2018JD029644

Grell, G. A., Peckham, S. E., Schmitz, R., McKeen, S. A., Frost, G., Skamarock, W. C., & Eder, B. (2005). Fully coupled "online" chemistry within the WRF model. *Atmospheric Environment, 39*(37), 6957-6975. http://www.sciencedirect.com/science/article/pii/S1352231005003560

Holben, B. N., Eck, T. F., Slutsker, I., Tanré, D., Buis, J. P., Setzer, A., et al. (1998). AERONET—A Federated Instrument Network and Data Archive for Aerosol Characterization. *Remote Sensing of Environment, 66*(1), 1-16. http://www.sciencedirect.com/science/article/pii/S0034425798000315

Hong, C.-C., Lu, M.-M., & Kanamitsu, M. (2008). Temporal and spatial characteristics of positive and negative Indian Ocean dipole with and without ENSO. *Journal of Geophysical Research: Atmospheres, 113*(D8). https://doi.org/10.1029/2007JD009151

Huffman, G. J. (1997). Estimates of Root-Mean-Square Random Error for Finite Samples of Estimated Precipitation. *Journal of Applied Meteorology, 36*(9), 1191-1201. https://doi.org/10.1175/1520-0450(1997)036<1191:EORMSR>2.0.CO;2

Huffman, G. J., Bolvin, D. T., Nelkin, E. J., Wolff, D. B., Adler, R. F., Gu, G., et al. (2007). The TRMM Multisatellite Precipitation Analysis (TMPA): Quasi-Global, Multiyear, Combined-Sensor Precipitation Estimates at Fine Scales. *Journal of Hydrometeorology, 8*(1), 38-55. https://doi.org/10.1175/JHM560.1

Hyer, E. J., & Chew, B. N. (2010). Aerosol transport model evaluation of an extreme smoke episode in Southeast Asia. *Atmospheric Environment, 44*(11), 1422-1427. http://www.sciencedirect.com/science/article/pii/S1352231010001020

Jimenez, J. L., Canagaratna, M. R., Donahue, N. M., Prevot, A. S. H., Zhang, Q., Kroll, J. H., et al. (2009). Evolution of Organic Aerosols in the Atmosphere. *Science, 326*(5959), 1525. http://science.sciencemag.org/content/326/5959/1525.abstract

Jin, Q., & Wang, C. (2017). A revival of Indian summer monsoon rainfall since 2002. *Nature Climate Change, 7*(8), 587-594. https://doi.org/10.1038/nclimate3348

Kaufman, Y. J., Tanré, D., & Boucher, O. (2002). A satellite view of aerosols in the climate system. *Nature, 419*(6903), 215-223. https://doi.org/10.1038/nature01091

Kumar, R., Naja, M., Pfister, G. G., Barth, M. C., & Brasseur, G. P. (2012). Simulations over South Asia using the Weather Research and Forecasting model with Chemistry (WRF-Chem): set-up and meteorological evaluation. *Geosci. Model Dev., 5*(2), 321-343. https://gmd.copernicus.org/articles/5/321/2012/

Kumar, R., Naja, M., Pfister, G. G., Barth, M. C., Wiedinmyer, C., & Brasseur, G. P. (2012). Simulations over South Asia using the Weather Research and Forecasting model with Chemistry (WRF-Chem): chemistry evaluation and initial results. *Geosci. Model Dev., 5*(3), 619-648. https://gmd.copernicus.org/articles/5/619/2012/

Lau, K.-M., & Kim, K.-M. (2006). Observational relationships between aerosol and Asian monsoon rainfall, and circulation. *Geophysical Research Letters, 33*(21). https://agupubs.onlinelibrary.wiley.com/doi/abs/10.1029/2006GL027546

Le, T., Wang, Y., Liu, L., Yang, J., Yung, Y. L., Li, G., & Seinfeld, J. H. (2020). Unexpected air pollution with marked emission reductions during the COVID-19 outbreak in China. *Science, 369*(6504), 702. http://science.sciencemag.org/content/369/6504/702.abstract

Lin, C., Cohen, J. B., Wang, S., & Lan, R. (2020). Application of a combined standard deviation and mean based approach to MOPITT CO column data, and resulting improved representation of biomass burning and urban air pollution sources. *Remote Sensing of Environment, 241*, 111720. http://www.sciencedirect.com/science/article/pii/S0034425720300894

Lin, C., Cohen, J. B., Wang, S., Lan, R., & Deng, W. (2020). A new perspective on the spatial, temporal, and vertical distribution of biomass burning: quantifying a significant increase in CO emissions. *Environmental Research Letters, 15*(10), 104091. http://dx.doi.org/10.1088/1748-9326/abaa7a

Lin, N.-H., Sayer, A. M., Wang, S.-H., Loftus, A. M., Hsiao, T.-C., Sheu, G.-R., et al. (2014). Interactions between biomass-burning aerosols and clouds over Southeast Asia: Current status, challenges, and perspectives. *Environmental Pollution, 195*, 292-307. http://www.sciencedirect.com/science/article/pii/S0269749114002838

Lin, N.-H., Tsay, S.-C., Maring, H. B., Yen, M.-C., Sheu, G.-R., Wang, S.-H., et al. (2013). An overview of regional experiments on biomass burning aerosols and related pollutants in Southeast Asia: From BASE-ASIA and the Dongsha Experiment to 7-SEAS. *Atmospheric Environment, 78*, 1-19. http://www.sciencedirect.com/science/article/pii/S1352231013003300

O'Neill, N. T., Eck, T. F., Smirnov, A., Holben, B. N., & Thulasiraman, S. (2003). Spectral discrimination of coarse and fine mode optical depth. *Journal of Geophysical Research: Atmospheres, 108*(D17). https://agupubs.onlinelibrary.wiley.com/doi/abs/10.1029/2002JD002975

Pan, X., Chin, M., Ichoku, C. M., & Field, R. D. (2018). Connecting Indonesian Fires and Drought With the Type of El Niño and Phase of the Indian Ocean Dipole During 1979–2016. *Journal of Geophysical Research:*

Atmospheres, 123(15), 7974-7988. https://agupubs.onlinelibrary.wiley.com/doi/abs/10.1029/2018JD028402

Pavagadhi, S., Betha, R., Venkatesan, S., Balasubramanian, R., & Hande, M. P. (2013). Physicochemical and toxicological characteristics of urban aerosols during a recent Indonesian biomass burning episode. *Environ Sci Pollut Res Int, 20*(4), 2569-2578.

Ramanathan, V., & Carmichael, G. (2008). Global and regional climate changes due to black carbon. *Nature Geoscience, 1*(4), 221-227. https://doi.org/10.1038/ngeo156

Reid, J. S., Hyer, E. J., Johnson, R. S., Holben, B. N., Yokelson, R. J., Zhang, J., et al. (2013). Observing and understanding the Southeast Asian aerosol system by remote sensing: An initial review and analysis for the Seven Southeast Asian Studies (7SEAS) program. *Atmospheric Research, 122*, 403-468. http://www.sciencedirect.com/science/article/pii/S0169809512001809

Reid, J. S., Koppmann, R., Eck, T. F., & Eleuterio, D. P. (2005). A review of biomass burning emissions part II: intensive physical properties of biomass burning particles. *Atmos. Chem. Phys., 5*(3), 799-825. https://acp.copernicus.org/articles/5/799/2005/

Reid, J. S., Xian, P., Holben, B. N., Hyer, E. J., Reid, E. A., Salinas, S. V., et al. (2016). Aerosol meteorology of the Maritime Continent for the 2012 7SEAS southwest monsoon intensive study – Part 1: regional-scale phenomena. *Atmos. Chem. Phys., 16*(22), 14041-14056. https://acp.copernicus.org/articles/16/14041/2016/

Reid, J. S., Xian, P., Hyer, E. J., Flatau, M. K., Ramirez, E. M., Turk, F. J., et al. (2012). Multi-scale meteorological conceptual analysis of observed active fire hotspot activity and smoke optical depth in the Maritime Continent. *Atmos. Chem. Phys., 12*(4), 2117-2147. https://acp.copernicus.org/articles/12/2117/2012/

Rosenfeld, D. (1999). TRMM observed first direct evidence of smoke from forest fires inhibiting rainfall. *Geophysical Research Letters, 26*(20), 3105-3108. https://agupubs.onlinelibrary.wiley.com/doi/abs/10.1029/1999GL006066

Rosenfeld, D., Andreae, M. O., Asmi, A., Chin, M., de Leeuw, G., Donovan, D. P., et al. (2014). Global observations of aerosol-cloud-precipitation-climate interactions. *Reviews of Geophysics, 52*(4), 750-808. https://agupubs.onlinelibrary.wiley.com/doi/abs/10.1002/2013RG000441

Sato, M., Hansen, J., Koch, D., Lacis, A., Ruedy, R., Dubovik, O., et al. (2003). Global atmospheric black carbon inferred from AERONET. *Proceedings of the National Academy of Sciences, 100*(11), 6319. http://www.pnas.org/content/100/11/6319.abstract

Schuster, G. L., Dubovik, O., Holben, B. N., & Clothiaux, E. E. (2005). Inferring black carbon content and specific absorption from Aerosol Robotic Network (AERONET) aerosol retrievals. *Journal of Geophysical Research: Atmospheres, 110*(D10). https://agupubs.onlinelibrary.wiley.com/doi/abs/10.1029/2004JD004548

Singh, N., Banerjee, T., Raju, M. P., Deboudt, K., Sorek-Hamer, M., Singh, R. S., & Mall, R. K. (2018). Aerosol chemistry, transport, and climatic implications during extreme biomass burning emissions over the Indo-Gangetic Plain. *Atmos. Chem. Phys., 18*(19), 14197-14215. https://acp.copernicus.org/articles/18/14197/2018/

Stavrakou, T., Müller, J. F., Boersma, K., De Smedt, I., & van der A, R. (2008). Assessing the distribution and growth rates of NOx emission sources by inverting a 10-year record of NO2 satellite columns. *Geophys. Res. Lett., 35*, 2-6.

Stone, E. A., Schauer, J. J., Pradhan, B. B., Dangol, P. M., Habib, G., Venkataraman, C., & Ramanathan, V. (2010). Characterization of emissions from South Asian biofuels and application to source apportionment of carbonaceous aerosol in the Himalayas. *Journal of Geophysical Research: Atmospheres, 115*(D6). https://agupubs.onlinelibrary.wiley.com/doi/abs/10.1029/2009JD011881

Streets, D. G., Yarber, K. F., Woo, J.-H., & Carmichael, G. R. (2003). Biomass burning in Asia: Annual and seasonal estimates and atmospheric emissions. *Global Biogeochemical Cycles, 17*(4). https://agupubs.onlinelibrary.wiley.com/doi/abs/10.1029/2003GB002040

Tang, W., Cohan, D. S., Lamsal, L. N., Xiao, X., & Zhou, W. (2013). Inverse modeling of Texas NO_x emissions using space-based and ground-based NO₂ observations. *Atmos. Chem. Phys., 13*(21), 11005-11018. https://acp.copernicus.org/articles/13/11005/2013/

Tao, W.-K., Chen, J.-P., Li, Z., Wang, C., & Zhang, C. (2012). Impact of aerosols on convective clouds and precipitation. *Reviews of Geophysics, 50*(2). https://agupubs.onlinelibrary.wiley.com/doi/abs/10.1029/2011RG000369

van der Werf, G. R., Dempewolf, J., Trigg, S. N., Randerson, J. T., Kasibhatla, P. S., Giglio, L., et al. (2008). Climate regulation of fire emissions and deforestation in equatorial Asia. *Proceedings of the National Academy of Sciences, 105*(51), 20350. http://www.pnas.org/content/105/51/20350.abstract

van der Werf, G. R., Randerson, J., Giglio, L., Leeuwen, T., Chen, Y., Rogers, B., et al. (2017). Global fire emissions estimates during 1997-2016. *Earth System Science Data, 9*, 697-720.

van der Werf, G. R., Randerson, J. T., Giglio, L., Collatz, G. J., Kasibhatla, P. S., & Arellano Jr, A. F. (2006). Interannual variability in global biomass burning emissions from 1997 to 2004. *Atmos. Chem. Phys., 6*(11), 3423-3441. https://acp.copernicus.org/articles/6/3423/2006/

Venzac, H., Sellegri, K., Laj, P., Villani, P., Bonasoni, P., Marinoni, A., et al. (2008). High frequency new particle formation in the Himalayas. *Proceedings of the National Academy of Sciences, 105*(41), 15666. http://www.pnas.org/content/105/41/15666.abstract

Wang, C. (2007). Impact of direct radiative forcing of black carbon aerosols on tropical convective precipitation. *Geophysical Research Letters, 34*(5). https://agupubs.onlinelibrary.wiley.com/doi/abs/10.1029/2006GL028416

Wang, C. (2013). Impact of anthropogenic absorbing aerosols on clouds and precipitation: A review of recent progresses. *Atmospheric Research, 122*, 237-249. http://www.sciencedirect.com/science/article/pii/S0169809512004231

Wang, S., Cohen, J. B., Lin, C., & Deng, W. (2020). Constraining the relationships between aerosol height, aerosol optical depth and total column trace gas measurements using remote sensing and models. *Atmos. Chem. Phys., 2020*, 1-24. https://acp.copernicus.org/preprints/acp-2019-1017/

Xue, L., Ding, A., Cooper, O., Huang, X., Wang, W., Zhou, D., et al. (2020). ENSO and Southeast Asian biomass burning modulate subtropical trans-Pacific ozone transport. *National Science Review*. https://doi.org/10.1093/nsr/nwaa132

Zaveri, R. A., Easter, R. C., & Peters, L. K. (2005). A computationally efficient Multicomponent Equilibrium Solver for Aerosols (MESA). *Journal of Geophysical Research: Atmospheres, 110*(D24). https://agupubs.onlinelibrary.wiley.com/doi/abs/10.1029/2004JD005618

Zaveri, R. A., Easter, R. C., & Wexler, A. S. (2005). A new method for multicomponent activity coefficients of electrolytes in aqueous atmospheric aerosols. *Journal of Geophysical Research: Atmospheres, 110*(D2). https://agupubs.onlinelibrary.wiley.com/doi/abs/10.1029/2004JD004681

Zhang, Q., Zheng, Y., Tong, D., Shao, M., Wang, S., Zhang, Y., et al. (2019). Drivers of improved PM_{2.5} air quality in China from 2013 to 2017. *Proceedings of the National Academy of Sciences, 116*(49), 24463. http://www.pnas.org/content/116/49/24463.abstract